J. Biochem. **144,** 159–166 (2008)
doi:10.1093/jb/mvn053

^{15}N NMR Relaxation Studies of Y14F Mutant of Ketosteroid Isomerase: The Influence of Mutation on Backbone Mobility

Hyeong Ju Lee[1], Ye Jeong Yoon[1], Do Soo Jang[2,*], Chul Kim[1,†], Hyung Jin Cha[2], Bee Hak Hong[2], Kwan Yong Choi[2,§] and Hee Cheon Lee[1,‡]

[1]Department of Chemistry; and [2]Division of Molecular Life Sciences, Pohang University of Science and Technology, Pohang, 790-784 Republic of Korea

Received March 4, 2008; accepted April 8, 2008; published online April 19, 2008

The backbone dynamics of Y14F mutant of Δ^5-3-ketosteroid isomerase (KSI) from *Comamonas testosteroni* has been studied in free enzyme and its complex with a steroid analogue, 19-nortestosterone hemisuccinate (19-NTHS), by ^{15}N NMR relaxation measurements. Model-free analysis of the relaxation data showed that the single-point mutation induced a substantial decrease in the order parameters (S^2) in free Y14F KSI, indicating that the backbone structures of Y14F KSI became significantly mobile by mutation, while the chemical shift analysis indicated that the structural perturbations of Y14F KSI were more profound than those of wild-type (WT) KSI upon 19-NTHS binding. In the 19-NTHS complexed Y14F KSI, however, the key active site residues including Tyr14, Asp38 and Asp99 or the regions around them remained flexible with significantly reduced S^2 values, whereas the S^2 values for many of the residues in Y14F KSI became even greater than those of WT KSI upon 19-NTHS binding. The results thus suggest that the hydrogen bond network in the active site might be disrupted by the Y14F mutation, resulting in a loss of the direct interactions between the catalytic residues and 19-NTHS.

Key words: backbone dynamics, ketosteroid isomerase, mutant, NMR, relaxation.

Abbreviations: CPMG, Carr–Purcell–Meiboom–Gill multi-pulse sequence; HSQC, heteronuclear single-quantum coherence; KSI, ketosteroid isomerase; 19-NTHS, 19-nortestosterone hemisuccinate; NMR, nuclear magnetic resonance; NOE, nuclear Overhauser effect; WALTZ, wideband alternating-phase low-power technique for zero residual splitting; WATERGATE, water suppression by gradient-tailored excitation; WT, wild-type.

Protein dynamics is a subject of great interest since it can greatly influence some important aspects of protein functions such as folding, stability and enzymatic reaction. In particular, the catalysed reaction of enzyme inherently involves dynamic processes with conformational changes, which are as important with respect to its function as the average structural properties (*1*). Thus, studies on the changes in protein dynamics upon mutation or ligand binding could be essential to understand the molecular interactions in catalysis or specific ligand binding of proteins (*2*).

Heteronuclear NMR has been widely used to describe the dynamics of proteins (*3*, *4*) since ^{13}C and ^{15}N NMR relaxation measurements can provide unique experimental data for the side chain and the backbone dynamics in a wide range of time scales from pico- to milliseconds. The model-free analysis (*5*, *6*) for heteronuclear relaxation data such as T_1, T_2, and nuclear Overhauser effect (NOE) provides dynamical information on the protein motions in terms of the overall correlation time for tumbling motions (τ_m), the generalized order parameter (S^2), the effective correlation time for internal motions (τ_e) and the conformational exchange contribution (R_{ex}). Dynamics studies by NMR thus have been applied to a large number of protein systems including the ligand-bound (*7–9*) and mutant (*10–12*) proteins.

Δ^5-3-ketosteroid isomerase (KSI) from *Comamonas testosteroni* is a homodimeric enzyme of 26.8 kDa (125 amino acid residues per monomer) with six-stranded β-sheets and three α-helices in each cone-shaped monomer (Fig. 1), which catalyses the isomerization of a variety of Δ^5-3-ketosteroids to Δ^4-3-ketosteroids *via* a dienolic intermediate with diffusion-controlled rate. Three-dimensional structures of KSI from *C. testosteroni* both in solution and crystal states have been identified by NMR and X-ray crystallography (*13*, *14*). A hydrogen bond network was found to have a large importance on the maintenance of the proper active site geometry for both function and stability of KSI (*15*), which connects two critical catalytic residues, Tyr14 and Asp99, with Phe30, Tyr55 and a water molecule in the highly apolar active site (*16*). In the catalytic process of KSI, Tyr14 plays a crucial role by formation of a direct hydrogen bond to C3 oxygen of the dienolate intermediate (*17*). It has been reported that the k_{cat} value was dramatically decreased by *ca.* 10^4-fold for Y14F mutant of *C. testosteroni* KSI relative to that for the wild-type (WT) enzyme (*18*). A number of NMR

*Present address: The J. David Gladstone Institute, SF, CA94158, USA
†Present address: 012 Fairchild Library, Division of Chemistry and Chemical Engineering, Caltech, Pasadena, CA91125, USA
§Correspondence may also be addressed. Tel: +82-54-279-2295, Fax: +82 54 279 2199, E-mail: kchoi@postech.ac.kr
‡To whom correspondence should be addressed. Tel: +82-54-279-2116, Fax: +82 54 279 3399, E-mail: hcl@postech.ac.kr

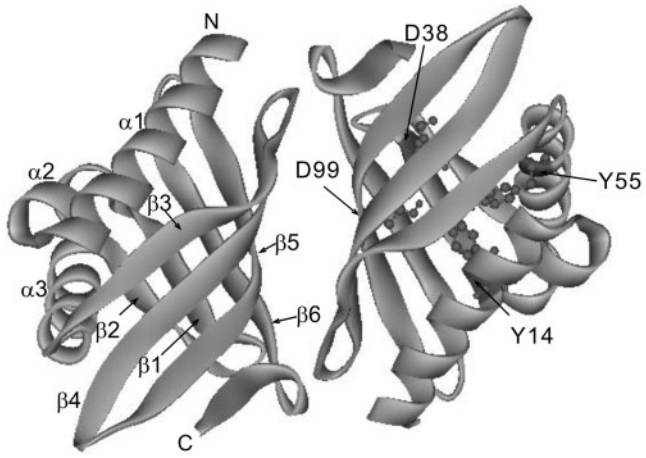

Fig. 1. **Crystal structure of dimeric KSI viewed roughly along the molecular 2-fold axis.**

relaxation studies on the backbone or side chain dynamics of *C. testosteroni* KSI have been carried out for better understanding the nature of enzymatic reaction (*19–21*). Thus, Zhao *et al*. (*19*) examined the side chain and backbone dynamics of the catalytic residue, Tyr-14, in a mutant KSI, Y55F/Y88F, by ^{13}C NMR relaxation measurements in the presence and absence of a steroid analogue, 19-nortestosterone hemisuccinate (19-NTHS), while Yun *et al*. (*20*, *21*) investigated the backbone dynamics of WT KSI by ^{15}N NMR relaxation measurements in free enzyme and its complex with 19-NTHS. However, no solution or crystal structures of Y14F KSI and no information on its dynamics are available at present presumably due to the instability of Y14F mutant, even though they could provide detailed information about the mutation-induced structural changes in local area as well as their propagation throughout the whole protein.

In order to further elucidate the role of Tyr14 in the enzyme activity and the maintenance of the optimum structure of *C. testosteroni* KSI, we have investigated the complete backbone dynamics of the single-point mutant (Y14F) of KSI in free enzyme and its complex with 19-NTHS by using ^{1}H-detected ^{15}N NMR relaxation measurements. Using the model-free analysis for the experimentally obtained ^{15}N T_1, ^{15}N T_2 and ^{15}N{^{1}H} NOE, the motional parameters such as S^2, τ_e and R_{ex} were extracted for the free and 19-NTHS complexed Y14F KSI. In addition, the differences in dynamics between the WT and Y14F KSI were discussed on the basis of structural features of the enzyme. The results indicate that the Y14F single mutation could disrupt the hydrogen bond network in the active site, leading to a loss of direct interactions between the catalytic residues and the steroid ligand, which may account for the dramatically reduced catalytic activity of Y14F KSI.

MATERIALS AND METHODS

Preparation of Labelled Y14F KSI—Mutant Y14F KSI was prepared by use of the Quickchange site-directed mutagenesis kit (Stratagene Inc.) using themocycler (MJ research). Expression vector, pKK-KSI (carrying the WT KSI gene) was used as a template with a set of two primers designed to encode desired mutation site in the KSI gene. Recombinant plasmids were transformed into *Escherichia coli* XL-1Blue supercompetent cells (Stratagene Inc.), and purified from the transformants by using Qiagen miniprep kit (Qiagen Inc.). The complete sequence of the gene was determined by the ABI 370 system (Applied Biosystem Inc.). Expression and purification of ^{15}N-labelled Y14F was performed as previously described (*20*).

NMR Samples—NMR samples were prepared to contain *ca*. 0.7 mM uniformly ^{15}N-labelled protein in 20 mM potassium phosphate, 10% (v/v) DMSO-d_6 and 90% H_2O. The pH of the sample was adjusted to 7.0. To obtain the steroid-bound protein, 19-NTHS pre-dissolved in DMSO-d_6 due to its insolubility in water, was added to the protein solution with a slightly excess amount relative to that of the protein, and then free unbound steroid was separated by ultra-centrifugation. The equilibrium constant (K_U) and the free energy change (ΔG_U) for the denaturation of KSI samples were determined with a two-state model by utilizing the following equations as described previously (*15*);

$$K_U = 2P_T\left[\frac{F_U 2}{(1-F_U)}\right] \quad (1)$$

$$\Delta G_U = -RT \cdot \ln(K_U) = \Delta G_U^{H_2O} - m\,[\text{urea}] \quad (2)$$

where P_T is the total protein concentration, F_U the apparent fraction of the unfolded form, $\Delta G_U^{H_2O}$ the free energy change in the absence of urea, and m a measure of dependency of ΔG_U on urea concentration.

NMR Measurements and Processing—All NMR data were collected at 300 K on a Bruker DRX500 spectrometer (500.13 MHz for ^{1}H and 50.7 MHz for ^{15}N) equipped with a triple resonance probe and pulsed-field *z*-gradient capability. The ^{15}N relaxation parameters T_1, T_2 and steady-state ^{15}N{^{1}H} NOE were measured by the standard pulse sequences (*22*, *23*) with WATERGATE (*24*) technique for the suppression of water resonance. Decoupling of ^{15}N spins during acquisition was performed using the GARP composite pulse sequence. The ^{1}H chemical shifts were calibrated with the internal chemical shift reference, sodium 2,2-dimethyl-2-silapentane-5-sulphonate. Indirect referencing method was used for the determination of ^{15}N chemical shifts (*25*). The cross-peak intensities were measured as peak volumes for better sensitivity, and the severely overlapped resonances were ruled out from the measurement of the relaxation parameters. A 4 s relaxation delay was used between scans for all experiments.

The T_1 and T_2 measurements were performed using a total of 96 transients per t_1 experiment. A total of $128 \times 2{,}048$ complex points were acquired in the $t_1 \times t_2$ dimensions. ^{15}N T_1 relaxation times were measured with delays of 28, 170, 340, 570, 1,020 and 1,500 ms. ^{15}N T_2 relaxation times were measured with delays of 5.6, 11.2, 28, 44.8, 56, 78.4 and 95.2 ms. The T_2 measurements utilized a 100 μs delay between sequential ^{15}N pulses in the CPMG pulse train for attenuating the ^{15}N signal loss during a T_2 relaxation period. To suppress undesirable effects of cross-correlation between ^{1}H-^{15}N dipolar and ^{15}N chemical shift anisotropy relaxation mechanisms in

the T_1 and T_2 experiments, GARP decoupling and ^{1}H inversion pulses were applied during the recovering delays as described (*20*). T_1 and T_2 values were calculated by non-linear regression of single exponential decays to the experimental data. The error levels in the T_1 and T_2 values were estimated by Monte Carlo simulations (*26*). The errors in the peak intensities for the simulation were determined from two independently measured relaxation data sets. Heteronuclear steady-state ^{15}N{^{1}H} NOE values were measured by calculating the ratio of the cross peak volumes in spectra recoded with and without ^{1}H saturation. The ^{1}H saturation was achieved by a train of 120° pulses separated by 5 ms for the relaxation delay. The NOE measurements were performed using a total of 96 transients per t_1 experiment.

Model-Free Analysis—^{15}N relaxation data were analysed with the model-free method (*5*, *6*) by using the program Modelfree v. 4.1 (*26*, *27*). An anisotropic model for rotational diffusion is essential in the case of highly asymmetric or multi-domain proteins. Dimeric KSI is highly asymmetric having a relative ratio of 1.00 : 0.95 : 0.55 for the principal components of the inertia tensor based on the solution structure (*13*). Our previous relaxation studies on the backbone dynamics of WT KSI also showed that the ^{15}N relaxation parameters were best described by an axially symmetric rotational diffusion tensor (*20*). Thus, an axially symmetric model was used to account for the overall rotational motion of the protein.

The molecular rotational diffusion tensor (**D**) was initially estimated from the measured T_1/T_2 values and the solution structure of free wt KSI (*13*) or Y55F/Y88F complexed with 19-NTHS (*19*) as input structures. The calculations were performed with the program Quadratic diffusion (*11*). The five models and the optimized parameters in each model were (*1*) S^2, (*2*) S^2 and τ_e, (*3*) S^2 and R_{ex}, (*4*) S^2, τ_e and R_{ex}, and (*5*) S_s^2, S_f^2 and τ_e, where S^2 is the generalized order parameter characterizing the amplitude of the internal motions, τ_e is the effective correlation time for the internal motions, R_{ex} is the exchange contribution to T_2, and the subscripts f and s indicate fast and slow time scales, respectively. The spectral density functions used for calculations of the relaxation data in an axially symmetric diffusion case are given by

$$J(\omega) = \frac{2}{5}\left[S^2 \sum_{j=1}^{3} \frac{A_j \tau_j}{1 + (\omega\tau_j)^2}\right] \quad (3)$$

$$J(\omega) = \frac{2}{5}\left[S^2 \sum_{j=1}^{3} \frac{A_j \tau_j}{1 + (\omega\tau_j')^2} + \frac{(1 - S^2)\tau}{1 + (\omega\tau)^2}\right] \quad (4)$$

$$J(\omega) = \frac{2}{5}\left[S^2 \sum_{j=1}^{3} \frac{A_j \tau_j}{1 + (\omega\tau_j)^2} + \frac{(S_f^2 - S^2)\tau}{1 + (\omega\tau)^2}\right] \quad (5)$$

where $\tau^{-1} = 6D + \tau_e^{-1}$, $\tau_1^{-1} = 6D_\perp$, $\tau_2^{-1} = 5D_\perp + D_\parallel$, $\tau_3^{-1} = 2D_\perp + 4D_\parallel$, $A_1 = (3\cos^2\theta - 1)^2/4$, $A_2 = 3\sin^2\theta\cos^2\theta$ and $A_3 = (3/4)\sin^4\theta$, and θ is the angle between the N–H bond vector and the principal axis of the diffusion tensor. D is the isotropic diffusion constant, and $D_\parallel$ and $D_\perp$ are the components of the diffusion tensor parallel and perpendicular to the principal axis of the axial symmetry, respectively (*20*). The isotropic correaltion time, can be newly defined and is related to the isotropic diffusion constant D by $\tau = (6D)^{-1}$. The parameter A_j, which reflects the orientation of the amide N–H vector with respect to the principal axis of the diffusion tensor, was estimated from the solution structure of free wt KSI (*13*) or Y55F/Y88F complexed with 19-NTHS (*19*) as input structures. Eqs 3–5 were used for models 1, 2 and 5, respectively, and additional R_{ex} term was introduced to the Eqs 3 and 4 for models 3 and 4. In model 5 (Eq. 5), $S^2 = S_s^2 S_f^2$, and the number of adjustable parameters is three for all five models, which can be extracted from the three experimental relaxation parameters. In the last stage of calculations, both the τ_m value and the $D_\parallel/D_\perp$ ratio were optimized simultaneously with all other model-free parameters.

RESULTS AND DISCUSSION

Effects of Steroid Binding on the Local Structures of Y14F KSI—The assignments of backbone amide ^{1}H and ^{15}N chemical shifts for Y14F KSI and its complex with 19-NTHS were easily achieved by comparing cross-peaks from the ^{1}H-^{15}N heteronuclear single-quantum coherence (HSQC) spectra with the published assignments of WT KSI (*20*). Comparison of the chemical shifts between free and complexed Y14F KSI indicates that there are large chemical shift changes upon ligand binding, which could be attributed to the local perturbations in the structural characteristics of mutant KSI by 19-NTHS ligand. In order to quantitatively evaluate the effect of ligand binding on the shift changes of amide group cross-peaks, the cumulative chemical shift differences ($\Delta\delta_{cum}$) were determined for each of the cross-peaks in ^{1}H-^{15}N HSQC spectrum according to the following equation (*28*):

$$\Delta\delta_{cum} = \left[(\Delta\delta_H)^2 + (\Delta\delta_N)^2\right]^{1/2} \quad (6)$$

where $\Delta\delta_N$ and $\Delta\delta_H$ denote chemical shift differences of cross-peaks between free and steroid-bound KSI measured in Hz for ^{1}H and ^{15}N dimensions, respectively. Figure 2 shows the $\Delta\delta_{cum}$ values for Y14F KSI as a function of residue number. Most of the residues with large shift changes upon ligand binding are located on the flexible regions such as loops or turns between secondary structures or terminal parts of the secondary structure elements. The global pattern of the chemical shift changes upon ligand binding for Y14F KSI is similar to that of WT KSI, however, the average $\Delta\delta_{cum}$ of 30.2 Hz for Y14F KSI is much larger than that of 19.7 Hz for the wt protein (*20*), indicating that the structural perturbations of Y14F KSI are more profound than that of WT KSI upon 19-NTHS binding. In addition, while a total of 12 residues such as Phe14, Ile51, Asn57, Lys60, Leu61, Ala64, Ala81, Glu87, Ile98, Asn104, Ala114 and His122 exhibit very large $\Delta\delta_{cum}$ values (over *ca.* 60 Hz, a sum of the average and standard deviation), a large part of them (4 out of 12) are relatively localized on the α3-helix. Since a ligand recognition, activation or binding affinity of proteins are known to accompany conformational changes of protein chain (*29*, *30*), the chemical shift changes of Y14F KSI

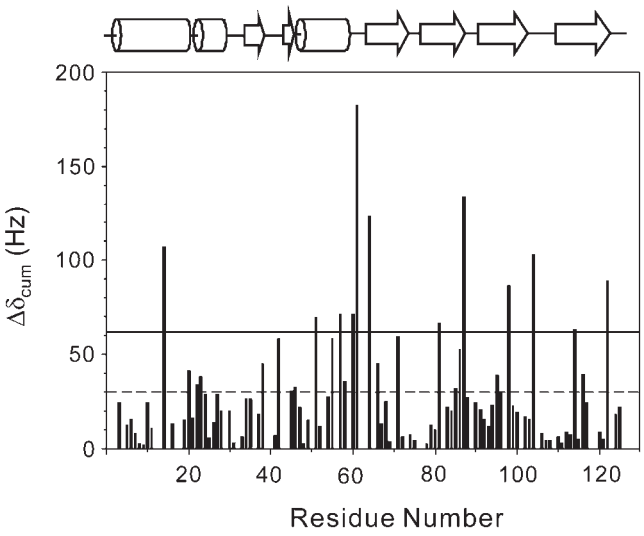

Fig. 2. **Cumulative chemical shift differences between the free and 19-NTHS complexed Y14F KSI as a function of residue number.** The solid and dashed horizontal lines represent a specific cut-off (the sum of average and standard deviation) and an average value of chemical shift differences, respectively. The secondary structure elements of WT KSI determined by X-ray crystallography are depicted on top of the figure; α-helices are marked with cylinders, and β-strands are with arrows.

upon 19-NTHS binding might be attributed to such conformational changes. In this context, it is interesting to note the results from previous study on the solution structures of free and 19-NTHS bound KSI from *C. testosteroni* that the binding of 19-NTHS with enzyme induced a movement of three α-helices, which became more closely packed onto the concave surface of the β-sheet (*31*).

Backbone Dynamics of Free Y14F KSI—Among the 120 residues in KSI which can yield backbone amide signals (excluding the N-terminal methionine and four proline residues), 24 residues were excluded from the analysis because of severe resonance overlap or poor signal intensity. Thus, quantitative ^{15}N relaxation measurements were carried out for 96 amide cross-peaks in the ^{1}H-^{15}N HSQC spectrum of free Y14F KSI. For most residues, the T_1 and T_2 values lie in the range of 0.9–1.5 s and 35–60 ms, respectively, while the heteronuclear ^{15}N{^{1}H} NOEs are in the range of 0.6–0.9. The two C-terminal residues (Gly124 and Ala125) or the residues in the linker regions between secondary structure elements exhibit significantly lower NOE values presumably due to their high mobility.

Since it has been shown in our previous study on the backbone dynamics of WT KSI that the ^{15}N relaxation parameters were best described by an axially symmetric rotational diffusion tensor (*20*), the model-free analysis for Y14F KSI was also performed with an axially symmetric one. As a result, the overall rotational correlation time (τ_m) for free Y14F KSI was determined to be 20.08 ± 0.03 ns with a diffusion anisotropy, $D_{\parallel}/D_{\perp}$, of 1.19 ± 0.02, which is slightly larger than the τ_m value of 19.23 ± 0.07 ns for free WT KSI (*20*). The optimized model-free parameters, S^2, τ_e and R_{ex} are shown in Fig. 3A–C, and the spectral density models used to fit the ^{15}N NMR relaxation data are summarized in Table 1. Most of the residues have the S^2 values of >0.8, indicating that rapid motions on the picosecond time scale are highly restricted (*32*, *33*). The well-defined secondary structure elements, α-helices and β-strands, have the average S^2 values of 0.86 ± 0.02 and 0.82 ± 0.02, respectively, which are substantially smaller than the values of 0.95 ± 0.03 and 0.93 ± 0.03 for the free WT KSI (*20*), indicating that the backbone structures of Y14F KSI are significantly loosened by mutation. On the other hand, the S^2 values of <0.8 were observed from the residues that are located in the regions around β5-strand (Arg91–Phe103), terminus of secondary structure elements, and C-terminal. The effective correlation times (τ_e) for internal motions were detected for 15 residues. Among them, a total of six residues such as Ala73, Gly90, Arg91, Lys92, Gly124 and Ala125 showed large τ_e values >500 ps, which are located on the flexible regions with low S^2 values. The exchange term (R_{ex}), which could reflect the existence of a dynamic exchange process in the microsecond to millisecond time scale (*6*), was detected for 13 residues.

Dynamics of Complexed Y14F KSI and Effects of Steroid Binding—For the complexed Y14F KSI, ^{15}N relaxation measurements were carried out for 97 residues out of 120 measurable backbone amide groups. The changes in ^{15}N relaxation parameters of Y14F KSI upon 19-NTHS binding were very similar to those of WT KSI, where the T_1 values of the complexed KSI were slightly smaller than those of free protein, while the T_2 values were slightly larger for the complexed KSI.

The model-free analysis for the complexed Y14F KSI was also performed with an axially symmetric rotational diffusion tensor, and the overall rotational correlation time (τ_m) was determined to be 18.09 ± 0.03 ns with a diffusion anisotropy, $D_{\parallel}/D_{\perp}$, of 1.33 ± 0.01. This τ_m value was slightly smaller than that of 20.08 ± 0.03 ns for the free Y14F KSI, indicating some extent of shrinking of the protein upon 19-NTHS binding. This tendency of Y14F KSI to be compact upon ligand binding was also observed in the relaxation studies of backbone dynamics of WT KSI. Of course, there could be some systematic errors between the two sets of data for WT and Y14F KSI; however, we did make every effort to carry out the relaxation measurements of Y14F KSI under the same sample and experimental conditions that were used for WT KSI to avoid such errors. Nevertheless, the possibility of systematic errors between two data sets may not be completely ruled out. The optimized model-free parameters, S^2, τ_e and R_{ex} for the complexed Y14F KSI are shown in Fig. 3D–F, and the spectral density models used to fit the ^{15}N NMR relaxation data are summarized again in Table 1. Relaxation data for most residues are fitted well using a simple model (S^2 only or S^2 and τ_e). Most of the residues have the S^2 values of >0.8, indicating that the residues are located in the ordered regions with restricted internal mobility (*32*, *33*). The effective correlation times (τ_e) for internal motions were observed for 22 residues. Slower motions of τ_e on the time scale >500 ps were observed for the residues of Gly41, Gln89, Gly90, Arg91, Lys92, Gly124 and Ala125, which are mainly located on the flexible regions of KSI.

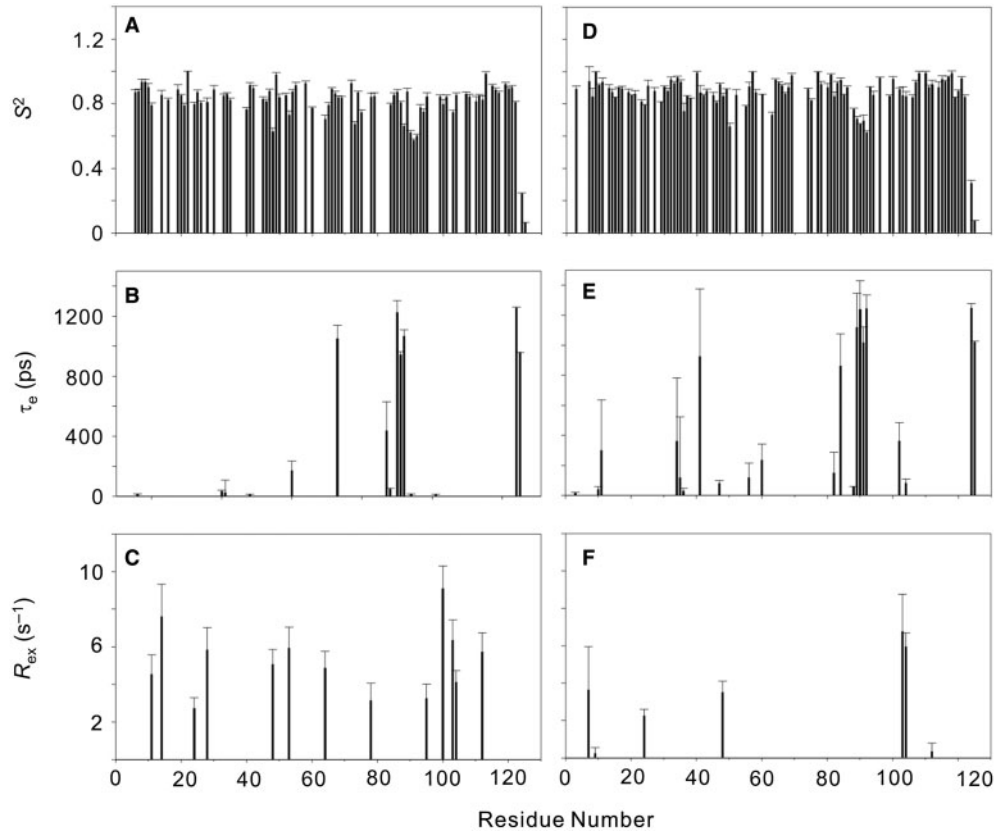

Fig. 3. **Plots of the model-free parameters and their uncertainties as a function of residue number for the free (A–C) and 19-NTHS complexed Y14F KSI (D–F).** (A, D) The generalized order parameter S^2. (B, E) The effective correlation time τ_e. (C, F) The chemical exchange contribution R_{ex}.

Table 1. **Summary of models used to fit ^{15}N T_1, T_2 and NOE data for free and 19-NTHS complexed Y14F KSI.**

Model no.	Model parameter	Number of residues	
		Free Y14F	Complexed Y14F
1	S^2	52	64
2	S^2 and τ_e	6	15
3	S^2 and R_{ex}	12	6
4	S^2, τ_e and R_{ex}	1	1
5	S_s^2, S_f^2 and τ_e	8	6
	Not fit	17	5
	Total	96	97

The number of residues fitted with R_{ex} was only seven, which is about half of the 13 residues for the free Y14F KSI, indicating that extremely slow motions on the micro- to millisecond time scale are more limited in the complexed Y14F KSI than in the free mutant.

The average S^2 values of α-helices and β-strands for the complexed Y14F KSI were 0.87 ± 0.02 and 0.89 ± 0.02, respectively, which are slightly larger than the values of 0.86 ± 0.02 and 0.82 ± 0.02 for the free Y14F KSI (*20*), indicating that the backbone structures of Y14F KSI become more rigid upon 19-NTHS binding. It seems that the loosened structures of Y14F KSI by mutation are partially tightened by plugging the active site cavity with a 19-NTHS steroid. Figure 4 shows the plot of the differences in S^2 between the free and complexed Y14F KSI as a function of residue number, where the order parameters for a majority of the residues are increased upon 19-NTHS binding. In particular, the β3-, β4- and

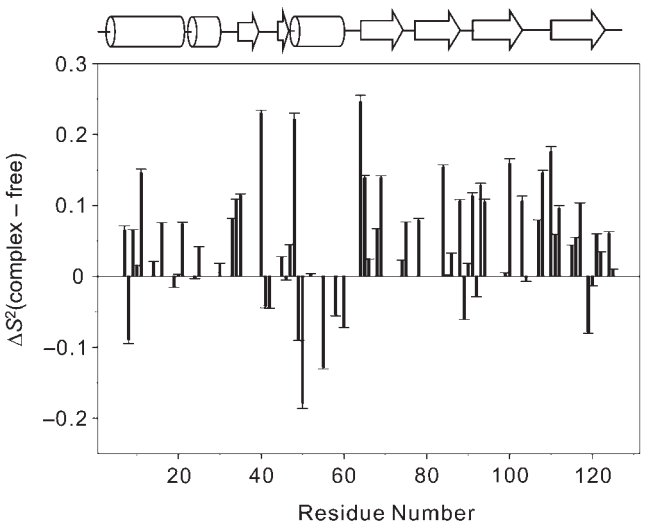

Fig. 4. **Plot of the differences in the order parameters (S^2) between the free and 19-NTHS complexed Y14F KSI.** Only the residues of which relaxation parameters were determined in both free and complexed proteins were included in this plot.

β5-strands become more rigid upon 19-NTHS binding, which happen to be involved in the formation of dimeric interface. Similar observations of increased order parameters upon ligand binding have been reported for a large number of protein systems, particularly the monomeric proteins (*9*, *33*, *34*). On the other hand, the rigidity of α3-helix is solely decreased upon ligand binding, which may have some correlations with the largest structural perturbations in α3-helix as monitored by the cumulative chemical shift changes in Fig. 1.

Effects of Mutation on the Backbone Dynamics of KSI—Figure 5 shows the plot of the differences in S^2 between the Y14F and WT KSI for free (A) and complexed (B) proteins as a function of residue number. It is evident from Fig. 5A that the S^2 values of free Y14F KSI are significantly smaller than those of WT KSI for most of the residues, indicating that the backbone structures of mutant KSI are more flexible than those of WT KSI. An equilibrium unfolding experiment on Y14F KSI using circular dichroism (CD) spectroscopy also showed that the mutant KSI was less stable than the WT protein. When the CD data were fitted to the two-state model (data not shown), the free energy difference, ΔG_U^{H2O}, and the m value of Y14F KSI were determined to be *ca*. 18.2 kcal/mol and 3.0 kcal/mol·M, respectively, which are significantly smaller than the values of *ca*. 22.0 kcal/mol and 4.0 kcal/mol·M for WT KSI (*35*). Thus, the Y14F KSI is less stable than the WT KSI by *ca*. 3.8 kcal/mol, which might support the observation that the backbone structures of Y14F KSI are more flexible than the WT KSI. Such a difference in flexibility and stability between the Y14F mutant and WT KSI can also be noticed from the HSQC spectra of the mutant (open circle) and WT (closed circle) proteins as shown in Fig. 5C, which were reconstructed using the reported chemical shifts of WT KSI (*20*) and those of Y14F mutant in this study (See Supplementary Data for ^{1}H and ^{15}N chemical shifts).

Contrary to the almost uniform decrease in S^2 in free Y14F KSI, the differences in S^2 between the Y14F and WT KSI for 19-NTHS complexed proteins vary along the sequence. As can be seen in Fig. 5B, three limited regions of Val10–Phe30, Val36–Gly47 and Phe80–Asp99 remained flexible with significantly reduced S^2 values upon 19-NTHS binding, while the S^2 values for many of the residues in the complexed Y14F KSI were similar to or even greater (more rigid) than those of WT KSI. It seems that the significantly loosened structures of free Y14F KSI are partially recovered by plugging the active site cavity with a 19-NTHS steroid, resulting in enhanced stability of complexed Y14F KSI compared to the free mutant, though the free energy difference ΔG_U^{H2O} was not measured due to low CD sensitivity of complexed Y14F KSI. Since the backbone dynamics of protein can be related to its function (*36*–*39*), the observed variations in ΔS^2 upon mutation for the complexed KSI might be expected to have a relationship with the enzymatic function of KSI. There are four active site residues such as Tyr14, Asp38, Tyr55 and Asp99 in WT KSI. It has been reported that the single-point mutations of these four residues such as Y14F, D38N, Y55F and D99L decreased the enzyme activity by about 10^4-, 10^6-, 6- and 10^2-fold, respectively (*15*, *40*). According to

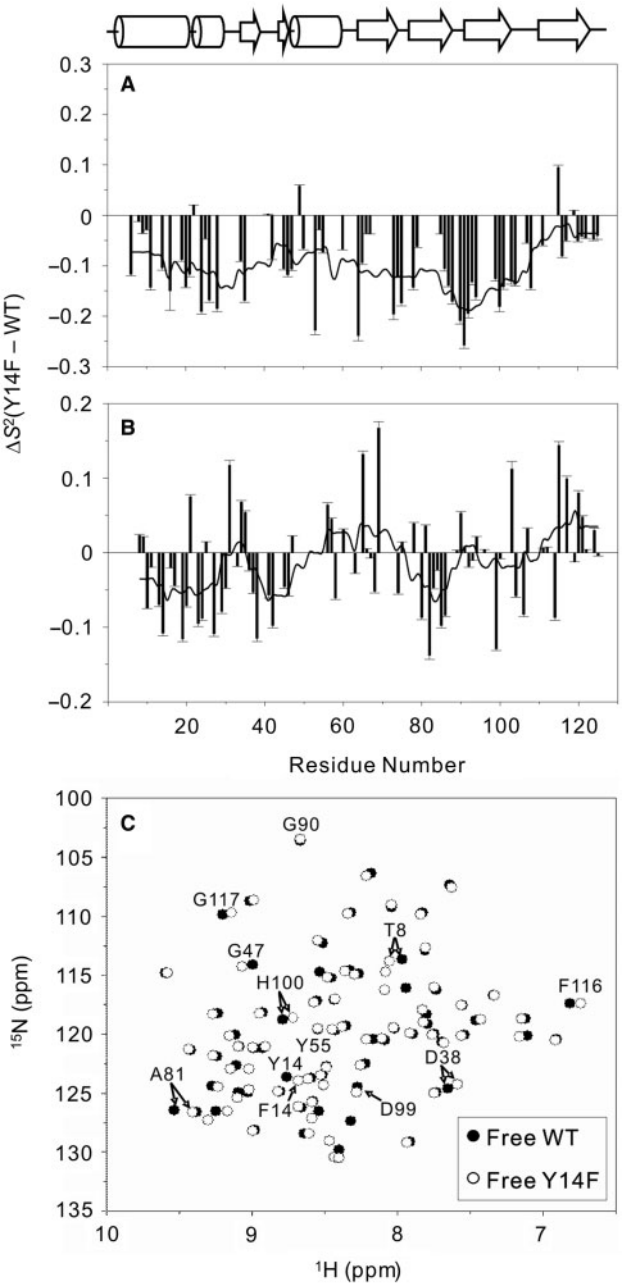

Fig. 5. **Plot of the difference in the order parameters (S^2) between the Y14F and wild-type KSI for (A) free and (B) 19-NTHS complexed proteins.** The solid line represents a smoothing of the data by averaging over five neighbouring points (centred on the point of interest). (C) Reconstructed HSQC spectra of the mutant (open circle) and WT (closed circle) proteins, which were reconstructed using the reported chemical shifts of WT KSI from ref. 20 and those of Y14F mutant in this study.

Ha *et al*. (*41*), the enzyme reactions of KSI exhibit the formation of low-barrier hydrogen bond between the steroid and the active site residues, in particular Tyr14 and Asp99. It is interesting to note that the region of Val10–Phe30 happens to contain the key catalytic residue of Tyr14 in the middle, whose flexibility might be attributed to the breakdown of the hydrogen bond

Table 2. **Order parameters (S^2) for the active site residues of wild-type and Y14F KSI.**

	S^2 (WT)[a]		S^2 (Y14F)	
Residue	Free	Complexed	Free	Complexed
Y14	0.96 ± 0.03	0.98 ± 0.02	0.85 ± 0.03	0.87 ± 0.02
D38	0.99 ± 0.02	0.95 ± 0.03	Not fit	0.83 ± 0.01
Y55	0.99 ± 0.02	Not fit	0.91 ± 0.02	0.78 ± 0.01
D99	0.97 ± 0.03	0.98 ± 0.02	0.84 ± 0.01	0.85 ± 0.01

[a]Values from Yun *et al.* (*20*).

between the OH group of Tyr14 and the C3 oxygen of the bound steroid caused by the Y14F mutation. More interestingly, the region of Val36–Gly47, which contains the most important catalytic residue of Asp38, also remains flexible upon ligand binding, even though it is far from the mutation point of Phe14. In fact, all the active site residues except Tyr55, whose S^2 values for WT KSI are not available for comparison, remain flexible with significantly reduced S^2 values upon 19-NTHS binding as can be seen in Table 2, while many of the residues in the complexed Y14F KSI become more rigid than those of complexed WT KSI as shown in Fig. 4B. The results thus suggest that the replacement of Tyr14 with Phe14 can cause a loss of the direct hydrogen bond between the protein and 19-NTHS due to substantially enhanced backbone flexibility of the protein, which may account for the dramatically reduced catalytic activity of Y14F KSI.

In summary, we have investigated the complete backbone dynamics of free Y14F KSI and its complex with 19-NTHS by ^{1}H-detected ^{15}N relaxation measurements. Model-free analysis of the relaxation data showed that the binding of 19-NTHS to free mutant KSI caused an increase in the order parameter (S^2) for most of the residues, particularly in the β-strands, while the chemical shift analysis of ^{1}H-^{15}N HSQC spectra indicated that the structural perturbations of Y14F KSI were more profound than those of WT KSI upon 19-NTHS binding. In addition, the Y14F single mutation caused a uniform decrease in S^2 in free KSI, while the S^2 changes upon mutation varied along the sequence in the complexed KSI. In particular, the key active site residues or the regions around them remained flexible with significantly reduced S^2 values even after the binding of 19-NTHS, indicating that the interactions in the active site are disrupted by the single mutation, which may account for the dramatically reduced catalytic activity of Y14F KSI. The results thus suggest that ^{15}N relaxation analysis of the backbone amides can be very useful for investigating the catalytic mechanism of enzymes in detail at residue level.

Supplementary data are available at *JB* Online.

This work was supported by the grants from POSTECH BSRI research fund (2004) and Korea Research Foundation (C00178).

REFERENCES

1. Osborne, M.J., Schnell, J., Benkovic, S.J., Dyson, H.J., and Wright, P.E. (2001) Backbone dynamics in dihydrofolate reductase complexes: role of loop flexibility in the catalytic mechanism. *Biochemistry* **40**, 9846–9859
2. Yu, L., Zhu, C.X., Tse-Dinh, Y.C., and Fesik, S.W. (1996) Backbone dynamics of the C-terminal domain of *Escherichia coli* topoisomerase I in the absence and presence of single-stranded DNA. *Biochemistry* **35**, 9661–9666
3. Palmer, A.G., III. (1997) Probing molecular motion by NMR. *Curr. Opin. Struct. Biol.* **7**, 732–737
4. Kay, L.E. (1998) Protein dynamics from NMR. *Nat. Struct. Biol.* **5 (7s)**, 513–517
5. Lipari, G. and Szabo, A. (1982) Model-free approach to the interpretation of nuclear magnetic resonance relaxation in macromolecules. 1. Theory and range of validity. *J. Am. Chem. Soc.* **104**, 4546–4559
6. Clore, G.M., Driscoll, P.C., Wingfield, P.T., and Gronenborn, A.M. (1990) Analysis of the backbone dynamics of interleukin-1β a using two-dimensional inverse detected heteronuclear ^{15}N-^{1}H NMR spectroscopy. *Biochemistry* **29**, 7387–7401
7. Yuan, P., Marshall, V.P., Petzold, G.L., Poorman, R.A., and Stockman, B.J. (1999) Dynamics of stromelysin/inhibitor interactions studied by ^{15}N NMR relaxation measurements: comparison of ligand binding to the S1-S3 and S'1-S'3 subsites. *J. Biomol. NMR* **15**, 55–64
8. Olejniczak, E.T., Zhou, M.M., and Fesik, S.W. (1997) Changes in the NMR-derived motional parameters of the insulin receptor substrate 1 phosphotyrosine binding domain upon binding to an interleukin 4 receptor phosphopeptide. *Biochemistry* **36**, 4118–4124
9. Zhang, W., Smithgall, T.E., and Gmeiner, W.H. (1998) Self-association and backbone dynamics of the hck SH2 domain in the free and phosphopeptide-complexed forms. *Biochemistry* **37**, 7119–7126
10. Adams, P.D., Loh, A.P., and Oswald, R.E. (2004) Backbone dynamics of an oncogenic mutant of Cdc42Hs shows increased flexibility at the nucleotide-binding site. *Biochemistry* **43**, 9968–9977
11. Shipp, E.L., Cantini, F., Bertini, I., Valentine, J.S., and Banci, L. (2003) Dynamic properties of the G93A mutant of copper-zinc superoxide dismutase as detected by NMR spectroscopy: implications for the pathology of familial amyotrophic lateral sclerosis. *Biochemistry* **42**, 1890–1899
12. Gorbatyuk, V.Y., Tsai, C.K., Chang, C.F., and Huang, T.H. (2004) Effect of N-terminal and Met23 mutations on the structure and dynamics of onconase. *J. Biol. Chem.* **279**, 5772–5780
13. Wu, Z.R., Ebrahimian, S., Zawrotny, M.E., Thornburg, L.D., Perez-Alvarado, G.C., Brothers, P., Pollack, R.M., and Summers, M.F. (1997) Solution structure of 3-oxo-Δ^5-steroid isomerase. *Science* **276**, 415–418
14. Cho, H.S., Choi, G., Choi, K.Y., and Oh, B.H. (1998) Crystal structure and enzyme mechanism of Δ^5-3-ketosteroid isomerase from *Pseudomonas testosteroni*. *Biochemistry* **37**, 8325–8330
15. Kim, D.H., Jang, D.S., Nam, G.H., Choi, G., Kim, J.S., Ha, N.C., Kim, M.S., Oh, B.H., and Choi, K.Y. (2000) Contribution of the hydrogen-bond network involving a tyrosine triad in the active site to the structure and function of a highly proficient ketosteroid isomerase from *Pseudomonas putida* biotype B. *Biochemistry* **39**, 4581–4589
16. Jang, D.S., Cha, H.J., Cha, S.S., Hong, B.H., Ha, N.C., Lee, J.Y., Oh, B.H., Lee, H.S., and Choi, K.Y. (2004) Structural double-mutant cycle analysis of a hydrogen bond network in ketosteroid isomerase from *Pseudomonas putida* biotype B. *Biochem. J.* **382**, 967–973
17. Xue, L.A., Talalay, P., and Mildvan, A.S. (1991) Studies of the catalytic mechanism of an active-site mutant (Y14F) of Δ^5-3-ketosteroid isomerase by kinetic deuterium isotope effects. *Biochemistry* **30**, 10858–10865
18. Kuliopulos, A., Talalay, P., and Mildvan, A.S. (1990) Combined effects of two mutations of catalytic residues on

the ketosteroid isomerase reaction. *Biochemistry* **29**, 10271–10280
19. Zhao, Q., Abeygunawardana, C., and Mildvan, A.S. (1996) ^{13}C NMR relaxation studies of backbone and side chain motion of the catalytic tyrosine residue in free and steroid-bound Δ^5-3-ketosteroid isomerase. *Biochemistry* **35**, 1525–1532
20. Yun, S., Jang, D.S., Kim, D.H., Choi, K.Y., and Lee, H.C. (2001) ^{15}N NMR relaxation studies of backbone dynamics in free and steroid-bound Δ^5-3-ketosteroid isomerase from *Pseudomonas testosteroni*. *Biochemistry* **40**, 3967–3973
21. Yun, S., Jang, D.S., Choi, G., Kim, K.S., Choi, K.Y., and Lee, H.C. (2002) Trifluoroethanol increases the stability of Δ^5-3-ketosteroid isomerase. ^{15}N NMR relaxation studies. *J. Biol. Chem.* **277**, 23414–23419
22. Barbato, G., Ikura, M., Kay, L.E., Pastor, R.W., and Bax, A. (1992) Backbone dynamics of calmodulin studied by ^{15}N relaxation using inverse detected two-dimensional NMR spectroscopy: the central helix is flexible. *Biochemistry* **31**, 5269–5278
23. Kay, L.E., Torchia, D.A., and Bax, A. (1989) Backbone dynamics of proteins as studied by ^{15}N inverse detected heteronuclear NMR spectroscopy: application to staphylococcal nuclease. *Biochemistry* **28**, 8972–8979
24. Piotto, M., Saudek, V., and Sklenar, V. (1992) Gradient-tailored excitation for single-quantum NMR spectroscopy of aqueous solutions. *J. Biomol. NMR* **2**, 661–665
25. Wishart, D.S., Bigam, C.G., Yao, J., Abildgaard, F., Dyson, H.J., Oldfield, E., Markley, J.L., and Sykes, B.D. (1995) ^{1}H, ^{13}C and ^{15}N chemical shift referencing in biomolecular NMR. *J. Biomol. NMR* **6**, 135–140
26. Palmer, A.G., III., Rance, M., and Wright, P.E. (1991) Intramolecular motions of a zinc finger DNA-binding domain from xfin characterized by proton-detected natural abundance ^{13}C heteronuclear NMR spectroscopy. *J. Am. Chem. Soc.* **113**, 4371–4380
27. Mandel, A.M., Akke, M., and Palmer, A.G., III. (1995) Backbone dynamics of Escherichia coli ribonuclease HI: correlations with structure and function in an active enzyme. *J. Mol. Biol.* **246**, 144–163
28. Gröger, C., Moglich, A., Pons, M., Koch, B., Hengstenberg, W., Kalbitzer, H.R., and Brunner, E. (2003) NMR-spectroscopic mapping of an engineered cavity in the I14A mutant of HPr from Staphylococcus carnosus using xenon. *J. Am. Chem. Soc.* **125**, 8726–8727
29. Lu, Z.L., Gallagher, R., Sellar, R., Coetsee, M., and Millar, R.P. (2005) Mutations remote from the human gonadotropin-releasing hormone (GnRH) receptor-binding sites specifically increase binding affinity for GnRH II but not GnRH I: evidence for ligand-selective, receptor-active conformations. *J. Biol. Chem.* **280**, 29796–29803
30. Ayers, S.D., Nedrow, K.L., Gillilan, R.E., and Noy, N. (2007) Continuous nucleocytoplasmic shuttling underlies transcriptional activation of PPARγ by FABP4. *Biochemistry* **46**, 6744–6752
31. Massiah, M.A., Abeygunawardana, C., Gittis, A.G., and Mildvan, A.S. (1998) Solution structure of Δ^5-3-ketosteroid isomerase complexed with the steroid 19-nortestosterone hemisuccinate. *Biochemistry* **37**, 14701–14712
32. Bjorndahl, T.C., Andrew, L.C., Semenchenko, V., and Wishart, D.S. (2007) NMR solution structures of the Apo and peptide-inhibited human rhinovirus 3C protease (Serotype 14): structural and dynamic comparison. *Biochemistry* **46**, 12945–12958
33. Canales-Mayordomo, A., Fayos, R., Angulo, J., Ojeda, R., Martin-Pastor, M., Nieto, P.M., Martin-Lomas, M., Lozano, R., Gimenez-Gallego, G., and Jimenez-Barbero, J. (2006) Backbone dynamics of a biologically active human FGF-1 monomer, complexed to a hexasaccharide heparin-analogue, by ^{15}N NMR relaxation methods. *J. Biomol. NMR* **35**, 225–239
34. Okamura, H., Makino, K., and Nishimura, Y. (2007) NMR dynamics distinguish between hard and soft hydrophobic cores in the DNA-binding domain of PhoB and demonstrate different roles of the cores in binding to DNA. *J. Mol. Biol.* **367**, 1093–1117
35. Kim, D.H., Jang, D.S., Nam, G.H., Yun, S., Cho, J.H., Choi, G., Lee, H.C., and Choi, K.Y. (2000) Equilibrium and kinetic analysis of folding of ketosteroid isomerase from *Comamonas testosteroni*. *Biochemistry* **39**, 13084–13092
36. Ivanova, E.V., Kolosov, P.M., Birdsall, B., Kelly, G., Pastore, A., Kisselev, L.L., and Polshakov, V.I. (2007) Eukaryotic class 1 translation termination factor eRF1–the NMR structure and dynamics of the middle domain involved in triggering ribosome-dependent peptidyl-tRNA hydrolysis. *FEBS J.* **274**, 4223–4237
37. Shan, L., Tong, Y., Xie, T., Wang, M., and Wang, J. (2007) Restricted backbone conformational and motional flexibilities of loops containing peptidyl-proline bonds dominate the enzyme activity of staphylococcal nuclease. *Biochemistry* **46**, 11504–11513
38. Bhattacharya, N., Yi, M., Zhou, H.X., and Logan, T.M. (2007) Backbone dynamics in an intramolecular prolylpeptide-SH3 complex from the diphtheria toxin repressor, DtxR. *J. Mol. Biol.* **374**, 977–992
39. Filipp, F.V. and Sattler, M. (2007) Conformational plasticity of the lipid transfer protein SCP2. *Biochemistry* **46**, 7980–7991
40. Kim, S.W. and Choi, K.Y. (1995) Identification of active site residues by site-directed mutagenesis of Δ^5-3-ketosteroid isomerase from *Pseudomonas putida* biotype B. *J. Bacteriol.* **177**, 2602–2605
41. Ha, N.C., Choi, G., Choi, K.Y., and Oh, B.H. (2001) Structure and enzymology of Δ^5-3-ketosteroid isomerase. *Curr. Opin. Struct. Biol.* **11**, 674–678